Linear stability of multilayer plane Poiseuille flows of Oldroyd B fluids

P. Laure*, H. Le Meur†, Y. Demay*, J.C. Saut† and S. Scotto*

September 30, 2004

Abstract

The linear stability of plane Poiseuille flows of two and three-symmetric layer is studied. The fluids follow an Oldroyd-B differential constitutive equation and both asymptotic and numerical techniques are used. The influence of the viscosity and elasticity stratification as well as the layer thickness are largely analysed by using the additiveness between Newtonian and elastic terms which is shown in the asymptotic study. In such way, we have determined some general asymptotic stable arrangements at vanishing Reynolds number. It is also found that these arrangements remain stable with respect to moderate wavelength disturbances. Finally, their destabilization with an increase in the Reynolds number is considered and two distinct behaviors are pointed out which depend on the convexity of the Poiseuille velocity profile.

AMS : 76A10, 76E05, 35Q35

Keywords : viscoelastic fluids, interface, linear stability, multifluid flow, Arnoldi, Orr-Sommerfeld.

---

*Institut non-linéaire de Nice (UMR CNRS 129), Université de Nice, Sophia Antipolis, 06560 Valbonne, France

†Laboratoire d'Analyse Numérique et EDP (URA 760 CNRS), Université Paris-Sud, Bât. 425, 91405 Orsay Cedex, France

1 Introduction

The stability of multilayer Poiseuille flow (tube or parallel plates) has been recently studied by numerous authors due to the growing industrial importance of multilayer products in polymer processing. For example, food packaging commonly uses films formed of three, five or more layers in order to put together polymers having different optical, mechanical and barrier (to air or water) properties. In the industrial process, the polymers are molten in screw extruders, and then pushed through a feedblock and a flat die [1]. This process is limited by the onset in some conditions of a wavy instability deteriorating the quality of the film. Co-extrusion of two components has been also used in the fiber industry, whereas concentric coextrusion was motived by problems associated with the transportation of heavy viscous oild through long pipeline [2]. Various parameters such as viscosity, surface tension, viscoelasticity, density and gravity intervene on the destabilization mechanism. However it is worth noticing that in the processing of multilayer sheets, the ratios of viscosity and viscoelasticity are the more discriminant parameters.

This article is concerned with the linear stability of a plane Poiseuille flow of two viscoelastic fluids. Both fluids follow an Oldroyd-B differential constitutive equation. This law introduces the difference of normal stress $\sigma_{x,x} - \sigma_{y,y}$ considered as the characteristic feature of viscoelasticity of polymeric fluid. Stability under infinitesimal disturbances is investigated by the means of generalized Orr-Sommerfeld equations, in each layer. These equations are completed with equilibrium (namely the jump on the normal stress and velocity) and kinematic interface equations.

The linear stability is classically studied by the computation of the spectrum of the linearized operator about a basic flow. We restrict our computation to disturbances which are periodic in the direction of the flow motion. The sign of the real part of these eigenvalues gives the stability criterion and it depends on the various parameters of the problem , but also of spatial periodicity. In our problem two methods are mainly used: the **longwave** analysis which allows us to separate the kinenatic equation from the equations of motion. In this way, one gets under the Olroyd-B approximation an analytical formula giving the "interfacial" eigenvalue as a polynomial expression of parameters. However this asymptotic analysis has to be completed by a more general stability analysis or **moderate wavelength** analysis. This step introduces heavy numerical problems in the approximation of the spectrum. The difficulty mainly comes from the introduction of a continuous spectrum due to the viscoelastic behaviour of polymeric fluids [3]. So, this analysis requires accurate numerical analysis and several numerical methods can be used. Among them, the pseudospectral Tau method using an expansion of eigenvectors in Chebyschev polynomials is the most precise (see [4]). Finally, the discrete problem corresponds to generalized eigenvalue problem which is solved by an Arnoldi method [5].

We, now, review briefly previous works on the stability of Poiseuille/Couette multilayer flows

A) The two-layer Newtonian and quasi Newtonian Couette- Poiseuille flow. The longwave stability analysis of the two-layer flow of viscous fluids with different viscosities was studied by Yih ([6]). It was found that for both plane Couette and Poiseuille flows, stability is governed by a function of viscosity and thickness ratios m and ϵ, whatever the Reynolds number is. Moreover, he has also pointed out that some regions in the parameter plane (ϵ, m) are stable when the less viscous layer is the thinner ("thin layer effect"). Yiantsios and Higgins ([7]) have completed for Poiseuille flow the previous longwave analysis and have also taken into account moderate wavelength. Moreover, a shortwave analysis was introduced in order to analyze the effect of the surface tension. Charru and Fabre ([8]) have shown that, for longwaves and moderate surface tension, the nonlinear behavior at small amplitudes is given by a

Kuramoto-Sivashinky equation. They have also pointed out that the Poiseuille flow is stable if the basic velocity profile is convex. Khomami ([9, 10]) has studied the longwave stability and the effect of the converging channel for power law fluids. Pinarbasi and Liakopoulos ([11]) have computed stability of a two-layer Poiseuille flow of Carreau-Yasuda and Bingham-like fluids at moderate wavenumbers (using a Tau method and a QZ algorithm). The three-layer vertical flow was considered by Renardy ([12]) whereas the three-layer horizontal Poiseuille flow has been studied by Anturkar *et al.* ([13]). [13]).

B) The multilayer viscoelastic Couette-Poiseuille flow. Generalization of the longwave stability analysis of plane Couette flow has been carried out by Li [14] for Olroyd-B fluids, and by Waters and Keeley ([15]) for Olroyd-B fluids with a shear-dependent Carreau viscosity. Antukar *et al.* [16] have also examined the stability of the two- and three-layer viscoelastic Poiseuille flow with respect to longwave and moderate wavelength disturbances. Later Chen [17] has pointed out an error in the shear stress condition at the inferface used in these previous works. Moreover, he has shown for Couette flow that the jump of the normal stress arises in the interfacial instability. This author has also studied interfacial unstability due to elastic stratification in the concentric coextrusion of two viscoelastic fluids ([18]). The shortwave analysis of a two-layer Poiseuille flow of UCM fluids was considered by Renardy ([19]). Finally, the most complete results on the interfacial instability for Oldroyd-B liquids with constant and shear rate dependent viscosities are given by Su and Khomami ([20]). The influence of the die geometry has also been considered by these authors and this paper is in a way the starting point of our present study.

C) Experiments Han and Shetty ([21, 22]), Anturkar *et al.* ([23]) have published experimental results and considered industrial configurations. In particular, the influence of a convergent geometry was numerically studied by Anturkar *et al.* ([24]) using a Galerkin method and experimentally by Khomami and Wilson ([25]). Nevertheless, despite a great interest for this subject in recent past years, comparison with experiment is not clear. This is due to difficulties encountered in industrial or laboratory observations. One of the difficulties is due to encapsulation effect (the less viscous fluids tends to encapsulates the more viscous component and the thikness ratio do not remain constant in the transverse direction [1]). In the same manner, it is difficult to ensure a constant temperature along the die and the viscosity and elastic properties of each layer are not well known and homegenuous. Finally, characterization of irregular interface need a suitable optical apparatus and it not always possible to measured precisely the spacial and temporal periods of the perturbated interface (see photogaphs in [22]). One way to elimate such a difficulty is to impose external temporally regular disturbances at the interface [25].

The aim of this paper is to perform both longwave and moderate wavelength stability analysis in two different geometries. In the first one, both fluids are in contact with the wall. In the second one, one of the fluid is in contact with the upper and lower walls and the second fluid is symmetrically encapsulated. In this latter case, the geometry is assumed to be symmetric, the gravity is neglected and the stability with respect to varicose and sinuous perturbations is studied. In Section 2, we give the governing equations and the Poiseuille profile around which linear stability is performed. In Section 3, we perform the longwave stability analysis of the Poiseuille flow (it can be found for the Couette flow in [19, 17]), and give new explicit formulae. This allows us to provide areas of stable regions in the plane (ϵ, m) for vanishing Reynolds number. In this way, we identify some general asymptotically stable configurations which are destabilized by an increase of the Reynolds number. In Section 4, the influence of a moderate wavenumber on these stable regions is considered. The effect of surface tension S (which prevents a destabilization induced by short wave perturbations) on critical Reynolds number is also analysed.

2 Governing equations

2.1 The geometries

The stability analysis will be developped in two different geometries. The first one is a two-layer flow (Fig. 1a), labelled as case **A**. In this case each fluid is in contact with a wall. The first layer, located between $y = 0$ and $y = d_1$, is designated as region 1 and the second one, located between $y = d_1$ and $y = d_1 + d_2$, as region 2.

The second geometry is a three-layer flow with identical external fluids (Fig. 1b) and is labelled as case **B**. The same fluid is in contact with both walls and the other one flows in the core. This system is symmetric with respect to horizontal axis and the core layer ($y \in (-d_1, d_1)$) is designated as region 1. The upper and lower layers are designated as region 2 and have the same depth d_2. This configuration is expected to give close results to the concentric case and it has also been studied experimentally in [21, 22].

Each fluid has different rheological properties which are noted in the standart way; namelly the viscosity η_k, the relaxation time λ_k, the polymeric components α_k and the density ρ_k. Finally, the interface equations are $y_s = s\ d_1 + h_s(x,t)$ with $s = 1$ in the case **A** and $s = \pm 1$ in the case **B** (obviously, we have $h_s(x,t) = 0$ for the basic flow).

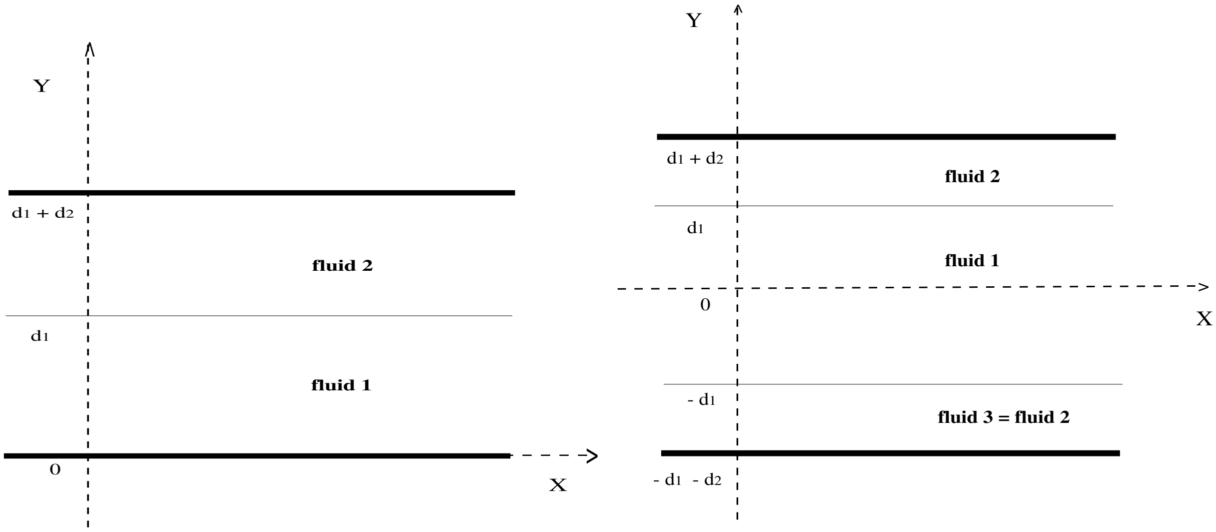

Figure 1: Geometries: (a) two-layer geometry; (b)three-symmetric layer geometry

2.2 The equations and stationary solutions

Let us denote $\underline{u}_k$ and $\underline{\underline{\tau}}_{p,k}$ the velocity field and viscoelastic extrastress in each layer. We assume that fluids are incompressible and obey an Oldroyd-B model. We choose the following space, velocity, time and stress scales,

$$d^* = d_1 \; ; \; U^* = U(y = d_1) \; ; \; t^* = \frac{d^*}{U^*} \; ; \; \sigma^* = \eta_1 \frac{U^*}{d^*}.$$

where U^* is the value of the Poiseuille velocity at the interface, Finally, the dimensionless equations in fluid k read as follows:

$$
\begin{aligned}
& r_k\mathrm{Re}\left(\frac{\partial \underline{u}_k}{\partial t}+(\underline{u}_k.\,\nabla)\ \underline{u}_k\right)+\nabla p_k-\ m_k\ (1-\alpha_k)\ \Delta\underline{u}_k\ =\nabla.\underline{\underline{\tau}}_{p,k}-\frac{r_k\ \mathrm{Re}}{F^2}\ \underline{e}_y,\\
& \underline{\underline{\tau}}_{p,k}\ +\ \ \mathrm{We}_k\ \left(\frac{\partial\underline{\underline{\tau}}_{p,k}}{\partial t}+\underline{u}_k.\nabla\underline{\underline{\tau}}_{p,k}-\nabla\underline{u}_k.\,\underline{\underline{\tau}}_{p,k}\ -\ \underline{\underline{\tau}}_{p,k}\ .\ \nabla\underline{u}_k^T\right)\ =\ \alpha_k\ m_k(\nabla\underline{u}_k\ +\ \nabla\underline{u}_k^T),\\
& \nabla.\underline{u}_k=0,
\end{aligned}
\tag{1}
$$

In the above equation, we exhibit the classical dimensionless parameters :
the Reynolds numbers $\mathrm{Re}=\rho_1U^*d_1/\eta_1$; the Weissenberg number $\mathrm{We}=\lambda_1\ U^*/d_1$ of fluid 1 ; the Froude number $F=U^*/\sqrt{gd_1}$; the ratio of viscosities $m=\eta_2/\eta_1$; the ratio of relaxation times $M_\lambda=(\alpha_2\ \lambda_2)/(\alpha_1\ \lambda_1)$; the ratio of densities $r=\rho_2/\rho_1$; the layer thickness ratio $\epsilon=d_2/d_1$; the surface tension number $S=T/\eta_1U^*$.

To simplify the notations in each layer, we have indexed by k the two Weissenberg numbers $\mathrm{We}_k=\lambda_k\ U^*/d^*$, the ratio of viscosities $m_k=\eta_k/\eta_1$ and the ratio of densities $r_k=\rho_k/\rho_1$. Let us notice that the problem has ten dimensionless parameters (Re, We, M_λ, α_1, α_2, m, r, S, F, ϵ) and that an infinite Froude number means that the vertical gravitational force is not taken into account.

This system of equation is completed by non-slip boundary condition,

$$
\begin{aligned}
& u_2(x,1+\epsilon)=v_2(x,1+\epsilon)=0,\\
& u_1(x,0)=v_1(x,0)=0\ \ \text{Case }\mathbf{A},\\
& u_2(x,-1-\epsilon)=v_2(x,-1-\epsilon)=0\ \ \text{Case }\mathbf{B},
\end{aligned}
\tag{2}
$$

and the interfacial conditions on the velocity and stress vector ($[\![f]\!]_s=s\ (f_1(s)-f_2(s))$ is the jump of a function f at the interface ($s=1$ or $s=\pm1$)) :

$$
\begin{aligned}
& [\![\underline{u}]\!]_s=0,\\
& [\![-p\underline{\underline{I}}+2(1-\alpha)m\underline{\underline{D}}[\underline{u}]+\underline{\underline{\tau}}_p]\!]_s\underline{n}=-2H\ S\underline{n},
\end{aligned}
\tag{3}
$$

where the vector $\underline{n}$ is a unit normal to the interface, $2H$ the sum of the principal curvatures. If we note $\underline{u}_k\ =\ (u_k,v_k)$ the velocity components, the immiscibility condition can be written as :

$$
\frac{\partial h_s}{\partial t}+u_1(y_s)\frac{\partial h_s}{\partial x}-v_1(y_s)=0.
\tag{4}
$$

Obviously in the above equation, the interface $s=-1$ is taken into account only for the three-layer case.

2.3 Basic flow

The multilayer Poiseuille flow is the x-invariant solution of equations (1-3). The velocity field is in each region :

$$
\text{case }\mathbf{A}:\ \ u_0(y)=\ -\frac{\epsilon\ +\ m}{m_k\ \epsilon\ (1\ +\ \epsilon)}\ y^2+\ \frac{m\ +\ 2\ \epsilon\ +\ \epsilon^2}{m_k\ \epsilon(1\ +\ \epsilon)}y+\ \frac{m_k\ -\ 1}{m_k},
\tag{5}
$$

$$
\text{case }\mathbf{B}:\ \ u_0(y)=\ -\frac{m}{m_k\ \epsilon(2+\epsilon)}y^2+\ 1\ +\ \frac{m}{m_k\ \epsilon(2+\epsilon)}.
\tag{6}
$$

The extrastress tensor $\begin{pmatrix} \sigma_0 & \tau_0 \\ \tau_0 & \gamma_0 \end{pmatrix}$ and the pressure p_0 are respectively, for each fluid:

$$\begin{aligned} \tau_0(y) &= m_k \; \alpha_k \; u_0', && (7) \\ \sigma_0(y) &= 2 \; m_k \; \alpha_k \;\; \mathrm{We}_k \; u_0'^2, && (8) \\ \gamma_0 &= 0, && (9) \\ p_0(x,y) &= -r_k \frac{\mathrm{Re}}{F^2} \; y \; + \; m_k \; u_0'' \; x \; + \mathcal{P}_0. && (10) \end{aligned}$$

The constant $\mathcal{P}_0$ is an arbitrary pressure, and prime $'$ designates $\partial/\partial y$.

2.4 Perturbation equations and interfacial eigenvalue

Since we are interested in the stability of the basic flow under infinitesimal perturbations and because of the x invariance, we classically introduce perturbations in the following form :

$$(\underline{u}_k, p_k, \underline{\underline{\tau}}_{p,k}, h_s) = (\tilde{\underline{u}}_k, \tilde{p}_k, \tilde{\underline{\underline{\tau}}}_{p,k}, \tilde{h}_s) \exp\,[iqx \; + \; \sigma t]. \tag{11}$$

The tilded variables, designating the amplitudes of disturbances, are (except the constant $\tilde{h}_s$) functions of y only. The number q is the wavenumber in the flow direction and σ is the frequency. Neglecting terms of order two in the amplitudes of the perturbations, we get the usual generalized Orr-Sommerfeld equations which can be found in [20, 17]. Non slip condition are imposed on the two walls, whereas at the interface ($y = s$) we get the same set of boundary conditions already written in [20, 17].

It is important to notice that the $y \to -y$ symmetry of the three-layer case, allows us to predict two possible unstable modes depending if this symmetry is preserved. Therefore, the symmetric solution is called the varicose mode ($h_{-1} = -h_1$) whereas the anti-symmetric solution is the sinuous mode ($h_{-1} = h_1$). Let us note that Hinch *et al.* [26] show that the sinuous mode can grow more rapidly than the varicose mode in the concentric coextrusion.

So, if we denote X the vector of coefficients of the Tchebichev expansion of each variable, we obtain, using a Tau method ([4]), a generalized eigenvalue problem of the following form :

$$A(q)\; X = \sigma\, B(q)\; X. \tag{12}$$

The matrices A and B are complex and B is singular. As usual, the stability of the basic flow is given by the sign of the real part of the generalized eigenvalues σ.

For a one-layer flow, the spectrum (the set of all the generalized eigenvalues) is well known. For example, the linear stability of Couette flow has been studied by Renardy & Renardy [27] for upper convected Maxwell fluid, whereas an Oldroyd-B model is considered for linear stability of Poiseuille flow by Sureshkumar and Beris in [3]. It is shown that the spectrum is constituted of a continuous spectrum and an infinite discrete spectrum. The destabilization come from an eigenvalue belonging to the discrete part of the spectrum and always occurs at high Reynolds numbers ($Re \sim 10^3$).

For a two-layer flow, the spectrum has the same general aspect as for a one-layer flow. The main feature [6] is that a new eigenvalue (referred as the interfacial eigenvalue) directly related to the interfacial equations and allows destabilization of the Poiseuille flow at small values of the Reynolds number. The critical Reynolds number is then a function of relevant parameters such as Weissenberg number, viscosity, elasticity and thickness ratios.

3 Long waves asymptotic analysis

In this section, we perform an asymptotic analysis in order to examine the stability of the interface under longwave ($q \to 0$) disturbances. To that purpose, we use a streamfunction ψ_k defined by $(u_k, v_k) = (\partial\psi_k/\partial y, -i\ q\ \psi_k)$ so that the divergence free condition is directly satisfied at each order. Following standart procedure [6], the streamfunction ψ and the growth rate σ are expanded in the form,

$$\psi = \psi^0 + q\psi^1 + q^2\psi^2 + \ ... \quad , \tag{13}$$

and

$$\sigma \ = \ -\, i\ q\ (c_0\ +\ q\ c_1\ +\ ...) \quad . \tag{14}$$

These expansions are substituted into the the whole system and terms of like order are grouped together. This way, we get a sequence of equations written in [7, 13] for Newtonians fluid and [18] for Maxwell fluid. We find that c_0 is real and c_1 purely imaginary. So, the stability is given by the sign of the real part of c_1 and $q\ c_0$ is the period of the perturbation, which is independent of the elastic properties. Finally the eigenvalues c_0 and c_1 are obtained with the help of the symbolic calculator MAPLE and written in a rather simple form :

$$c_0 \ = \ f(\epsilon, m) \text{ with } f \text{ real}, \tag{15}$$

$$\begin{aligned} c_1 \ = \ & i \text{ Re} \left(J_1(\epsilon, m) \ + \ (r-1) \left(J_2(\epsilon, m) \right) \ + \ \frac{J_3(\epsilon, m)}{F^2} \right) \\ & + i\ \alpha_1 \text{ We } \ (J_4(\epsilon, m) \ + (M_\lambda - 1)\ J_5(\epsilon, m)), \end{aligned} \tag{16}$$

where $M_\lambda = (\alpha_2\ \lambda_2)/(\alpha_1\ \lambda_1)$. The real functions J_1, J_2, J_3, J_4 and J_5 are given in Appendices A and B for the cases **A** and **B**.

From relation (16), it follows that the term c_1 is splitted into a Newtonian part (J_1, J_2 and J_3) and an elastic part (J_4 and J_5) and that the density stratification ($r \neq 1$) alters only the Newtonian part. Indeed, the stability will be a competition between the effects of all the controlling parameters with additiveness of all contributions except ε, m. Chen has also shown same kind of additiveness for the Couette flow [17] and the concentric coextrusion [18]. Nevertheless, this author has prefered to split the eigenvalue in a term proportional to $[\![u_0']\!]_s$ and another proportional to $[\![\sigma_0]\!]_s$.

In the case **A**, these functions satisfy symmetry properties which correspond to interchanging the fluid layers. The following relations are easily checked,

$$c_1(\frac{1}{\epsilon}, \frac{1}{m}, \frac{1}{r}) = \frac{m}{\epsilon^2}\ c_1(\epsilon, m, r) \quad \text{if} \quad \alpha_i = \text{We} = 0, \tag{17}$$

$$c_1(\frac{1}{\epsilon}, \frac{1}{m}, \frac{1}{M_\lambda}) = c_1(\epsilon, m, M_\lambda) \quad \text{if} \quad \text{Re} = 0, \tag{18}$$

Consequently, we limit the discussion to $M_\lambda > 1$ in the case **A**.

3.1 Stability of purely Newtonian fluids ($\mathbf{Re} \neq 0$ and $\mathbf{We} = 0$)

The case **A** has been studied by numerous authors [8, 7, 6, 13, 28] and we obtained basically the same results for the case **B**. Therefore, we only report here the main results. If we neglect the density stratification, equation (16) becomes :

$$c_1 = i \text{ Re } J_1(\epsilon, m). \tag{19}$$

The Poiseuille flow is stable if the function J_1 is negative. The expression of J_1 is given in Appendix A and B and we find that the Poiseuille flow is stable if the layer thickness of the less viscous fluid is small enough (lubricating effect). Moreover, J_1 has the opposite sign to the jump $[\![u_0']\!]$ in both cases **A** and **B**. So the remark about stable velocity profile given in [8] for two-layer Poseuille flow can be extended to the three symmetrical-layer case. That means that the process is stable when the basic velocity profile u_0 is convex. Examples of stable and unstable Poiseuille velocity profiles are plotted in Figs. 2 for the **A** and **B** cases.

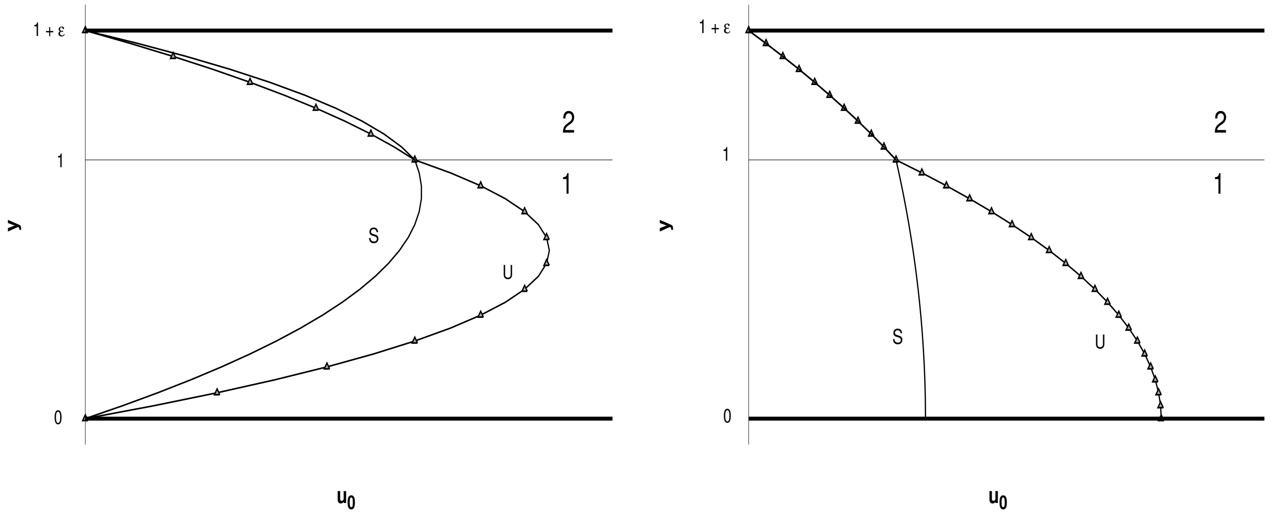

Figure 2: Stable and unstable velocity Poiseuille profiles u_0 in the case of purely Newtonian fluids: (a) two-layer Poiseuille flow; (b) three-layer Poiseuille flow

Finally, results about stable configurations of Newtonian flows can be summarized by the two following rules :
- the two-layer Poiseuille flow is stable when the thin layer is less viscous (Fig. 3a).
- The three-symmetric layer Poiseuille flow is stable when the more viscous fluid flows at core (Fig. 3b).

3.2 Stability of viscoelastic fluids ($\mathbf{We} \neq 0$ and $\mathbf{Re}= 0$)

Due to the high viscosity of polymer melts, we have to pay a particular attention to flows which are stable at vanishing Reynolds number.

When the viscosities are matched, $m = 1$, as $J_4(\epsilon, 1) = 0$, the stability is given by the sign of $(M_\lambda - 1)J_5(\epsilon, 1)$. The function $J_5(\epsilon, 1)$ is positive if $\epsilon < 1$ for the two-layer flow (case **A**) and if $\epsilon < \sqrt{2}$ for the varicose mode (case **B**) whereas it is always positive for sinuous mode. It is to notice that the corresponding value obtained by Chen ([18]) for the axisymmetric two-layer flow is $\epsilon = 1.7$. If $M_\lambda > 1$, the stable arrangements correspond to a larger upper layer for the case **A**, but the three symmetrical layer configuration is never stable because of the sinuous mode. If $M_\lambda < 1$, the outer layer has to be thinner for the case **B**. In these stable configurations, the layer closed to the wall is less elastic and thinner.

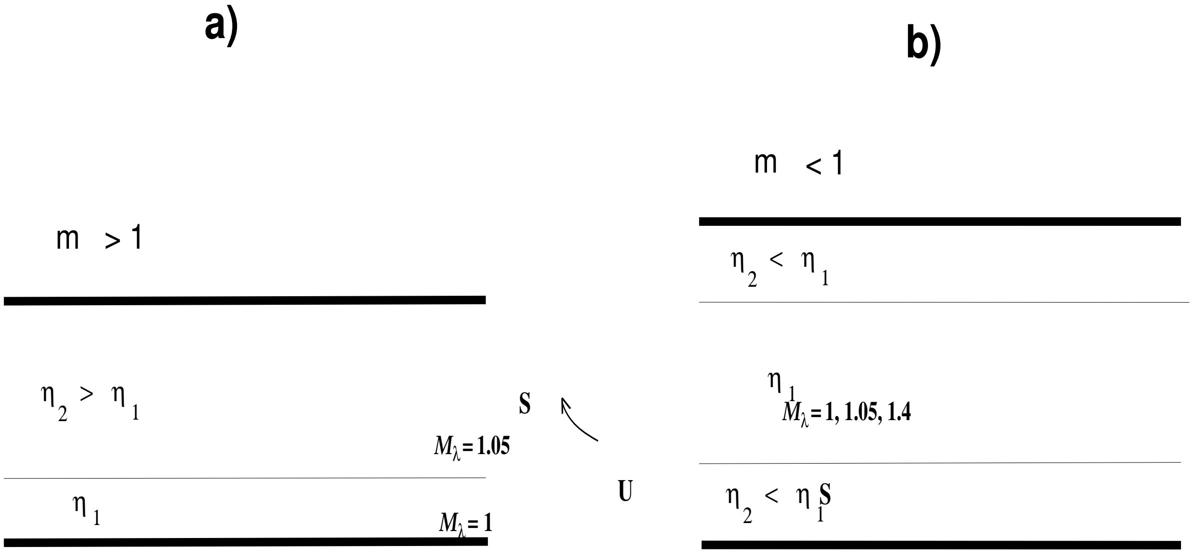

Figure 3: Sketches of stable situations for Newtonian fluids: (a) two-layer flow, $1 < m < \epsilon^2$; (b) three-layer flow, $m < 1$ and ϵ free, η_k is the viscosity of fluid k.

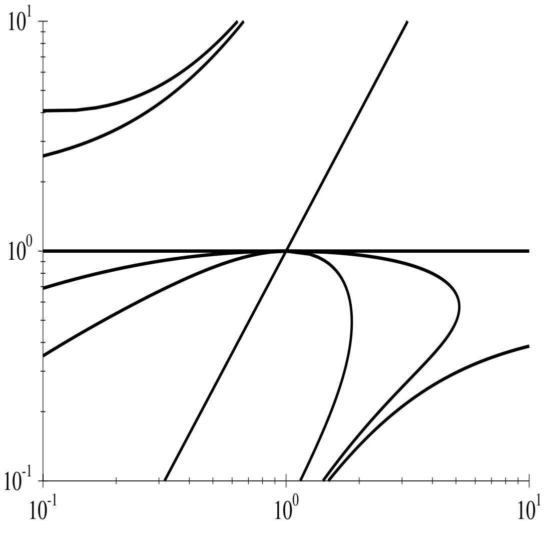

Figure 4: Two-layer case: Neutral curves $J_4 + (M_\lambda - 1)J_5 = 0$ in the plane (ϵ, m) for more elastic upper layer; $M_\lambda = 1., 1.05, 1.4$; The arrows indicate the displacement of the neutral curves with the relaxation time ratio M_λ

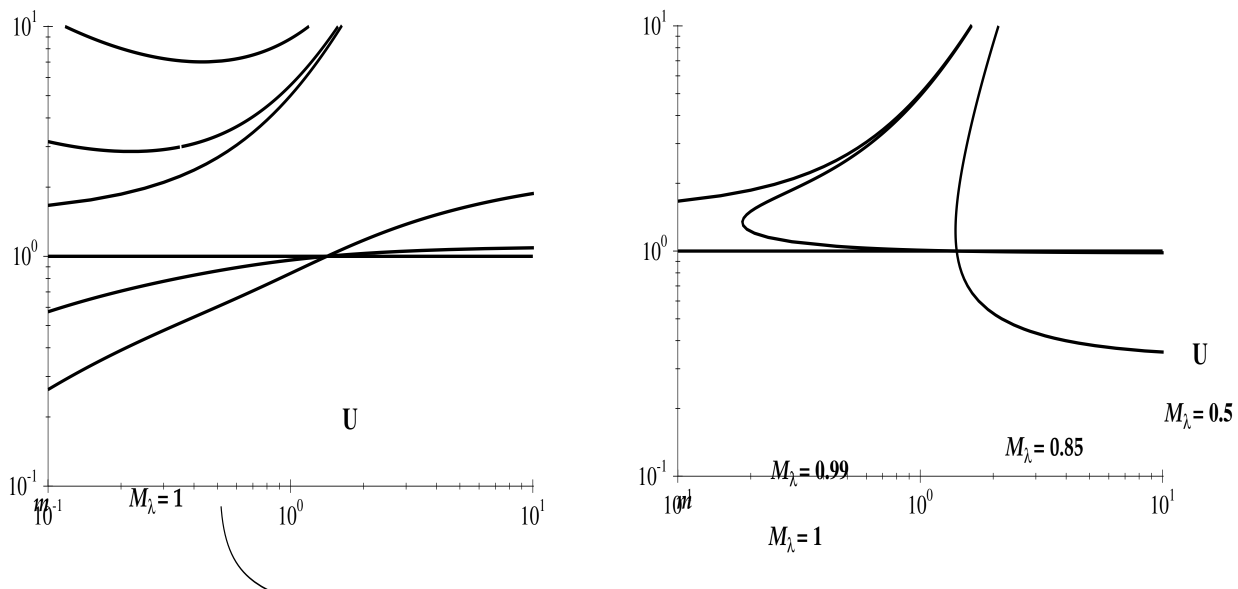

Figure 5: Varicose mode for three-symmetric layer case: Neutral curves $J4 + (M_\lambda - 1)J_5 = 0$ in the plane (ϵ, m) for various values of elastic stratification M_λ: (a) the core layer is less elastic, $M_\lambda = 1, 1.05, 1.4$; (b) the core layer is more elastic, $M_\lambda = 0.5, 0.99.1..$ The arrows indicate the displacement of the neutral curves with the relaxation time ratio M_λ

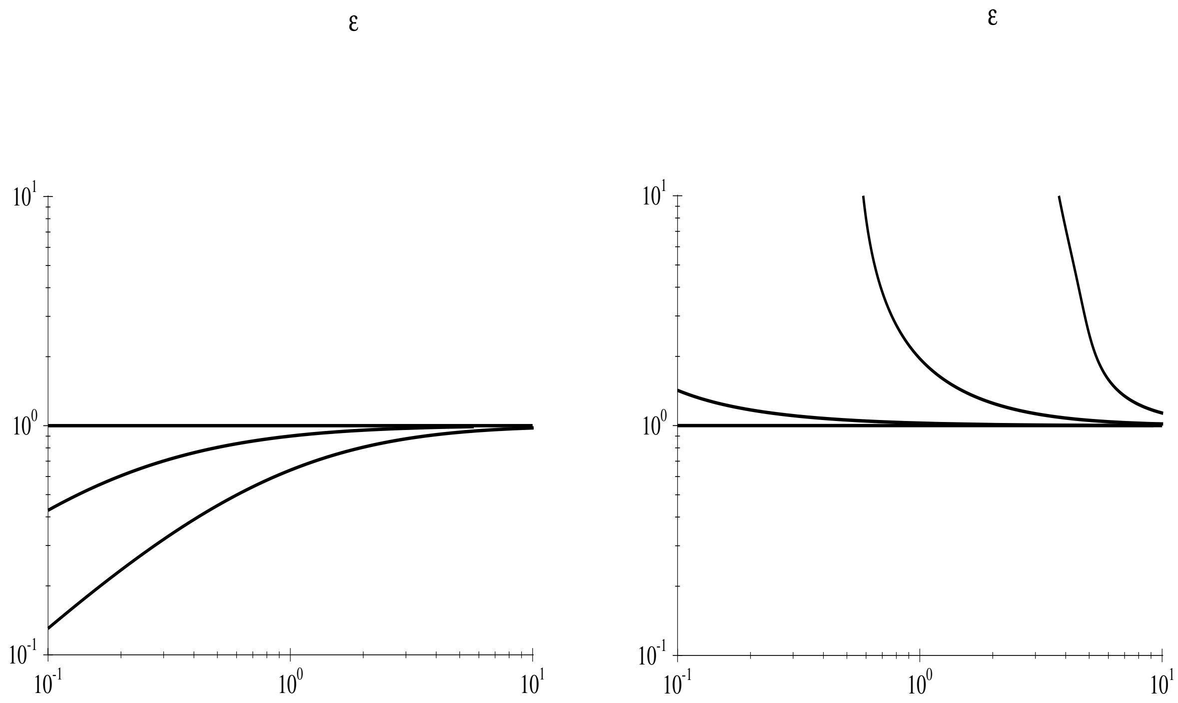

Figure 6: Sinuous mode for three-symmetric layer case: Neutral curves $J4 + (M_\lambda - 1)J_5 = 0$ in the plane (ϵ, m) for various values of elastic stratification M_λ: (a) the core layer is less elastic, $M_\lambda = 1, 1.05, 1.4$; (b) the core layer is more elastic, $M_\lambda = 0.5, 0.99.1..$ The arrows indicate the displacement of the neutral curves with the relaxation time ratio M_λ

When the viscosities are not matched ($m \neq 1$) we have to analyse the competition between viscous and elastic stratifications by means of functions J_4 and J_5. This effect can analyzed by means of Figs. 4, 5 and 6 in which the neutral curves of function $J_4 + (M_\lambda - 1)J_5$ are plotted for various values of M_λ.

The case **A** has widely been studied by Su and Khomami [20]. But, the additiveness of the relation (16) allows us to explain more clearly how to reach stable and unstable regions in the plane (ϵ, m). If the two fluids have the same elastic properties ($M_\lambda = 1$), we have once again four regions bounded by the curves $m = 1$ and $m = \epsilon^2$ with the same stability as in the purely Newtonian case. Moreover, there exist two other stable domains: the first one for small ϵ and large m and the second for large ϵ and small m. Therefore, the existence of these stable regions implies that the simple Charru's criterion on Poiseuille profile does not apply for Oldroyd-B fluids. Note also that these new domains can be eliminated by increasing the Reynolds number up to a critical one (as shown in Figs. 3a and 3b of [20]). The influence of elastic stratification ($M_\lambda \neq 1$) can be easily taken into account since J_5 has the sign of $m - \epsilon^2$ for all reasonnable values of$m$ and ϵ. If $M_\lambda > 1$, the elastic stratification acts as the Reynolds number in the upper mid-plane ($m > 1$) and the new stable region (observed for small ϵ and large m) can disappear. On other hand, the elastic stratification increases the stable region in the lower-mid plane ($m < 1$) and the stability becomes independant of m for sufficient big value of ϵ).

In the case **B** and for varicose perturbations, J_4 is negative for $m < 1$ or $1 + (1 + \epsilon)^3/2 < m$. Consequently, a configuration with a more viscous fluid in the core layer ($m < 1$) is again stable when $M_\lambda = 1$. Moreover, there exists a new stable region when the more viscous layer is outside ($m > 1 + (1 + \epsilon)^3/2$). So, if $M_\lambda > 1$, the elastic stratification acts again as the Reynolds number and the new stable region in the upper half plane $m > 1$ can disappear. Moreover, the half plane $m < 1$ can become unstable for small values of thickness ratio ϵ. If $M_\lambda < 1$, there exists a region for small values of ϵ which is stable for all values of viscosity stratification m. This means that if the outer layer is less elastic and thin enough, the Poiseuille profile is stable. This last result is similar to Chen's result in the case of concentric coextrusion (Fig. 5 in [18]). In conclusion, It seems that the two-layer interfacial mode and the varicose mode have the same behavior.

The action of the sinuous mode is simpler. If $M_\lambda = 1$, there is no difference with the Newtonian case (the mid-plane $m > 1$ is unstable, whereas the mid-plane $m < 1$ is stable). As seen in Figs. 6, if $M_\lambda < 1$ the mid-plane $m < 1$ is destabilized whereas if $M_\lambda > 1$, the mid-plane $m > 1$ becomes stable.

Experimental results are given in [22] for three and five layers. Concerning the three-layer flow and in agreement with the stability analysis, irregular interfaces are not observed if the more viscous fluid is sandwiched between the less viscous one (the LDPE/PS/LDPE system). On the contrary, unstable processing conditions are reported if the more viscous fluid is in contact with the wall (the PS/LDPE/PS system). The Figs. 15 and 16 in [22] show that unstable interfaces are obtained for a layer thickness ratio $h_{\mathrm{PS}}/h_{\mathrm{LDPE}}$ less than 0.8 when the viscosity ratio $\eta_{\mathrm{PS}}/\eta_{\mathrm{LDPE}} \sim 10$ and a normal stress difference ratio $(\sigma_1 - \sigma_2)_{\mathrm{PS}}/(\sigma_1 - \sigma_2)_{\mathrm{LDPE}} \sim 1$. With our parameters, that means that when $m = 10$ and $M_\lambda = 10.$, the flow will be unstable if $\epsilon < 1.6$. It is found from the longwave analysis at zero Reynolds number that the basic flow is unstable with respect to varicose perturbation if $\epsilon < 6.74$ whereas the sinuous perturbations is always destabilizing. We could explain the difference between experimental and our asymptotic analysis by a wrong choice of rheological behaviors. Both fluids have a shear-thinning or pseudoplastic behavior which corresponds to a power-law model $\eta = \eta_0 \, \partial_y u^{n-1}$ with $n_{\mathrm{PS}} = 0.33$ and $n_{\mathrm{LDPE}} = 0.45$. Moreover, the authors compute the viscosity ratio by taking for each fluid the viscosity at the wall when it is alone in the die. For a better comparison, more suitable values should be the viscosity ratio evaluated at the interface.

3.3 Asymptotically stable arrangements

The main results of this section are summarized in Fig. 7 where sketches of stable configurations for Re ~ 0 are drawn. Some of diagrams are deduced from stable arrangements depicted in Figs. 3 thanks to the additiveness of the various effects.

The three first arrangements correspond to the two and three-layer flows in which the elastic stratification reinforces the stability arising from the viscous stratification (Figs. 3a and 3b). As seen in Figs. 4, 5 and 6, this means generally that the more elastic layer has to be the larger one. For a two-layer flow, one may combine Fig. 3a (valid for $\epsilon > \sqrt{m}$) and $M_\lambda > 1$ to get Fig. 7a in which the larger layer is more viscous and more elastic. Whereas for a three-layer flow, one may similarly deduce the Figs. 7b and 7c from Fig. 3b (valid for all ϵ) by adjusting the two parameter M_λ and ϵ in a suitable way. Then, the more viscous core layer is either smaller and less elastic (Fig. 7b), or larger and more elastic (Fig. 7c).

The arrangements depicted in the two last Figs. 7d and 7e are different. In fact, the stability is due to the elastic properties which overcome the instability due to viscosity stratification. They correspond to the action of the function $(M_\lambda - 1)\ J_5$. For the two-layer flow, it can be seen in Fig. 4 that the larger layer has to be less viscous and more elastic (Fig. 7d). For the three-layer flow, the core layer is larger, less viscous and more elastic (Fig. 8e). As noted above, a Reynolds number amounts tends to destabilized this new stable regions. Therefore, it is possible to define an asymptotic critical Reynolds $\mathrm{Re}_o(q=0)$ from the formula (16) (the function J_1 is positive)

$$\mathrm{Re}_o(q=0) = -\alpha_1\ \mathrm{We}\ \frac{J_4(\epsilon,m) + (M_\lambda - 1)\ J_5(\epsilon,m)}{J_1(\epsilon,m)}, \tag{20}$$

which destabilize the two last arrangements.

In the next section, we check if these configurations remain stable for small and moderate wavelength disturbances when the Reynolds number vanishes.

4 Stability analysis for moderate wavelength

We discretized the eigenvalue problem for any disturbance wavelength q by using a Tau method [4]. The vector X is expanded in terms of Chebyschev polynomials of degree N. This leads to a generalized eigenvalue problem $(A - s\ B)X = 0$ where A and B are complex matrices of size $12 * N + 1$. The eigenvalue with the biggest real part is found by using an Arnoldi decomposition together with an inverse iterative method [29]. First, we checked that the numerical and asymptotic results are in excellent agreement.

Following the classical methodology, we look for stable and unstable regions in the $(\epsilon - q)$ plane when the rheological properties of the two fluids (namely m, M_λ, We and α_i) are fixed. Since we mainly focus our study on the competition between viscous and elastic effects, we take a zero Reynolds number Re, a null surface tension S, no density stratification ($r = 1$) and an infinite Froude number F. Numerical results are plotted in Figs. 8 and 9.

For a two layers flow (case **A**), we have chosen the parameters such that the two arrangements described in Figs 7a and 7d are recovered. The contour plotted in Fig. 8a ($m = 4.$; We $= .01$; $\alpha_k = .9$ and $M_\lambda = 1.2$) shows clearly that the stable asymptotic region occuring for $\epsilon > \sqrt{m}$ remains stable for higher values of the wavenumber q. In the same manner, we find from Fig. 8b ($m = 4.$; We $= .01$; $\alpha_k = .9$ and $M_\lambda = .8$) that the configuration with the more viscous and less elastic fluid in the thinner layer (diagram 7d) is stable when $\epsilon < .5$. Then, for a

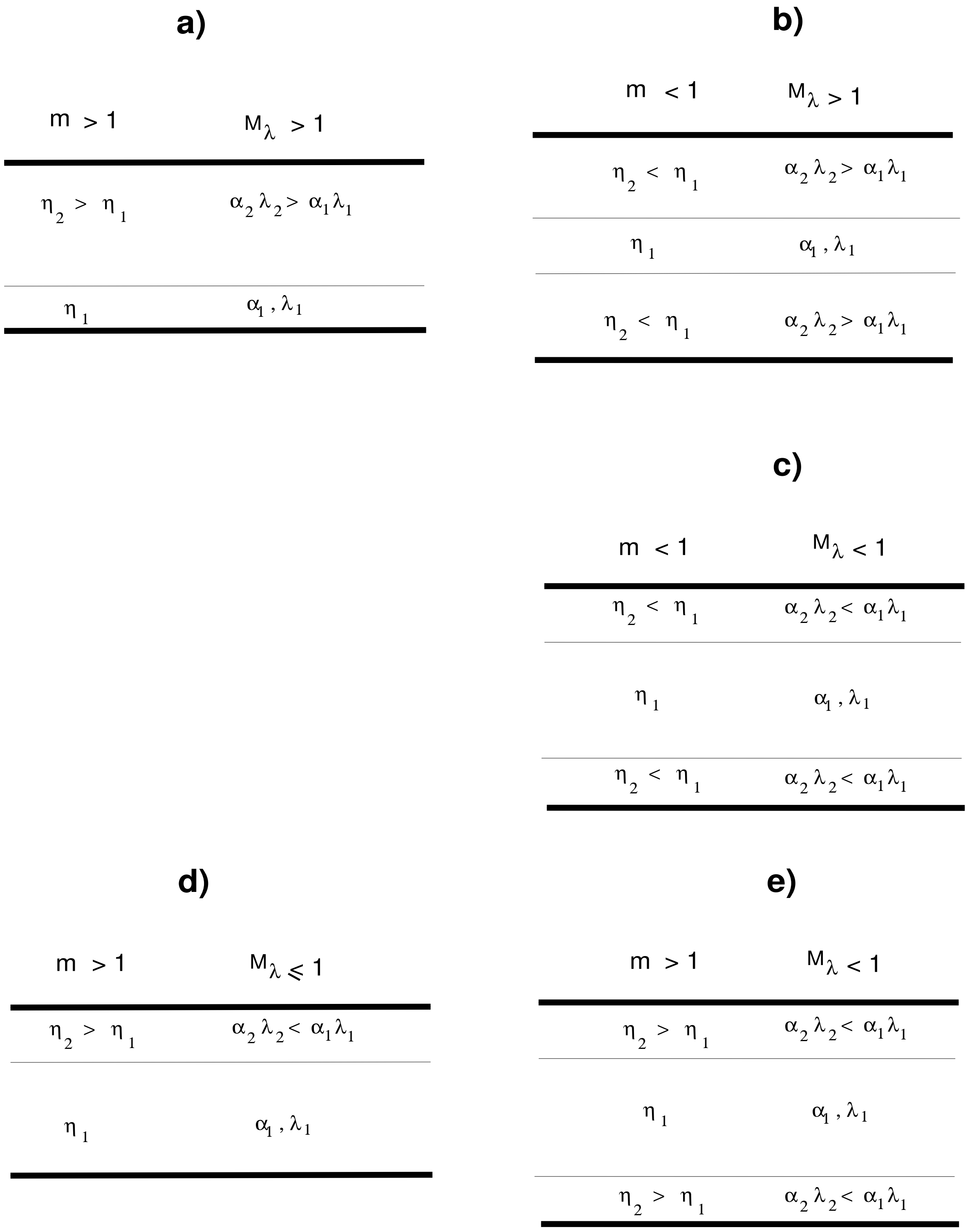

Figure 7: Sketches of asymptotic stable situations : (a) two-layer, $m > 1$, $M_\lambda > 1$, large ϵ; (b) three-layer, $m < 1$, $M_\lambda > 1$, large ϵ. (b) three-layer, $m < 1$, $M_\lambda < 1$, small ϵ. (d) two-layer, $m > 1$, $M_\lambda \leq 1$, small ϵ; (e) three-layer, $m > 1$, $M_\lambda < 1$, small ϵ; η_k, λ_k and α_k are respectively the viscosity, the relaxation time and polymeric component of fluid k

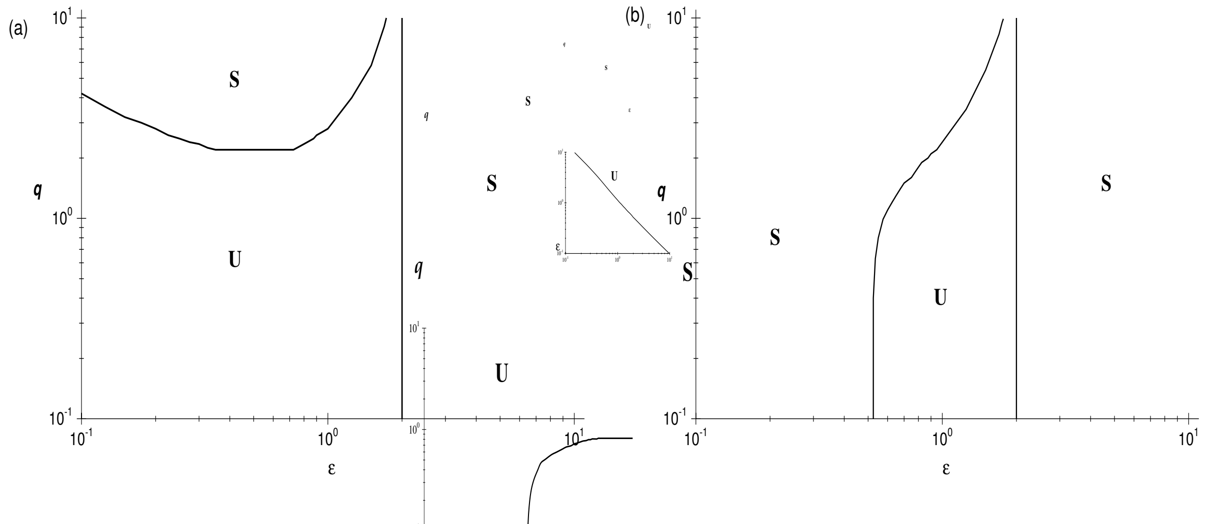

Figure 8: Moderate wavelength disturbances of two-layer flow. Neutral stability contours for Oldroyd-B fluids. Parameters: Re = 0, S = 0, $r = 1$, F = ∞, $\alpha_i = .9$, We = .01, $m = 4.$, (a) $M_\lambda = 1.2$; (b) $M_\lambda = .8$. Stable regions are denoted by S, unstable regions by U

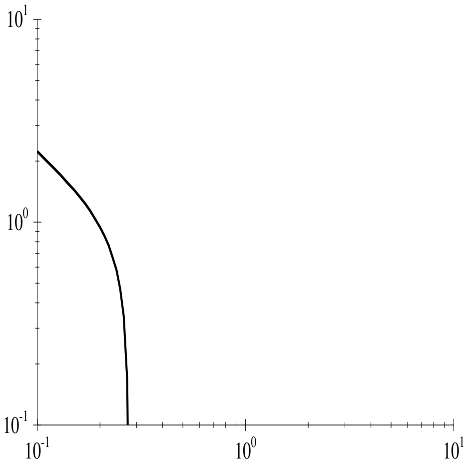

Figure 9: Moderate wavelength disturbances of three-symmetric layers. Neutral stability contours for Newtonian and Oldroyd-B fluids. Parameters: Re = 0, $S = 0$, $r = 1$, F = ∞, $\alpha_i = .9$, We = .01, (a) $m = .4$, $M_\lambda = 1.2$; (b) $m = 4.$, $M_\lambda = .8$. (c) Re = .1, $S = 0$, $r = 1$, $F = \infty$, α_k, We = 0, $m = .4$. Stable regions are denoted by S, unstable regions by U

small enough value of ϵ depending on viscous and elastic stratifications, this configuration is always stable. The second stable region of Fig. 8b found for $\epsilon > \sqrt{m}$ is not itemized in Figs. 7. In fact, the asymptotic neutral contours plotted in Fig. 4 shows that the stability of this arrangement is not insured for a smaller elastic stratification M_λ.

For a three-layer flow (case **B**), the computations exhibit the same kind of results. We have tested three examples of stable arrangements drawn in Figs. 7b, 7c and 7e. Neutral stability curves are plotted in Figs. 9a and 9b for a more viscous and less elastic core layer ($m = .4, M_\lambda = 1.2$) and a less viscous and more elastic core layer ($m = 4., M_\lambda = .8$) respectively. In this two figures, the curve delimiting the unstable area is giving by the sinuous mode Our computations show also that a situation with a more viscous and more elastic core layer ($m = .4, M_\lambda = .8$) remains stable for $.1 < q < 10$ whatever the thickness ratio ϵ.

Finally, we find that the eigenvalue σ is negative for all wavenumbers q in the range of thickness ratio found by the asymptotic analysis. Therefore, all the asymptotically stable configurations depicted in Figs. 7 remain stable with respect to moderate wavelength disturbances.

From these very specific computations, it seems possible to conclude that generally the asymptotic stability of configurations depicted in Figs. 8 induces a full stability when the Reynolds number is equal to zero. This result does not hold when $\mathrm{Re} \neq 0$ and for purely Newtonian fluids. For the two-layer Poiseuille flow (case **A**), we can forecast the effect of a non-zero Reynolds number on the stability thanks to Fig. 4 in [7] and Figs. 5, 6 and 7 in [20]. Firstly, for a sufficiently high Reynolds number, the arrangement with a larger more viscous fluid (Fig. 8a) is destabilized with a critical wavenumber of order unity. Secondly, the arrangement with larger less viscous fluid has a zero critical wavenumber. In the same manner for a three-layer flow (case **B**), the influence of a non-zero Reynolds number can be analyzed by means of Fig. 9d (where the neutral curve for a Newtonian fluid is plotted) and formula (20) because of the asymptotic stability for Newtonian fluid is driven by the function J_1. In particular, the Fig. 9c shows that the critical wavenumber will depend on the thickness ratio ϵ. It decreases from 10 to .1 as ϵ increases from .1 to 10 and this is a notable difference with respect to the two-layer case. Moreover, in this Fig. the unstable area is now bounded by the varicose mode. Notice also that the system where the low viscosity component is sandwiched between the high viscosity component can be destabilized by a longwave perturbation.

In order to describe more precisely the influence of the Reynolds number in both cases, we have determined the neutral Reynolds number Re_o as a function of the wavenumber q for fixed values of the thickness ratio ϵ. The neutral curves are plotted in Figs. 10 and Figs. 11 for the two-layer and the three-layer flows respectively. The critical wavenumber and Reynolds number are also given in the captions of these figures.

The two first Figs. 10a and 10b show in another way the difference behavior between Newtonian and viscoelastic fluid. In fact, if there is no superficial tension, the configuration becomes unstable in the Newtonian case as soon as the wavenumber is bigger than a critical value. This value does not depends on the Reynolds number. Nevertheless, if $S \neq 0$ (what is generally true) we get comparable picture to viscoelastic fluid and a critical Reynolds number can be exhibited.

The Figs. 10b, 11c and 11b show that the asymptotic analysis does not detect the destabilization by a Reynolds number increase for the three arrangements in Figs. 8a, 8b and 8c. This critical wavenumber is of order unity for two-layer flow (case **A**) whereas it decreases with the thickness ratio for the three-layer system (case **B**). This is in agreement with the above remark about the Fig. 9d. Moreover, the Figs. 9b, 11b and 11b show that the critical Reynolds number related to order one critical wavenumber increases quickly with the dimensionless surface tension S. On the other hand, the Figs. 10c and 11c point out that the asymptotic analysis

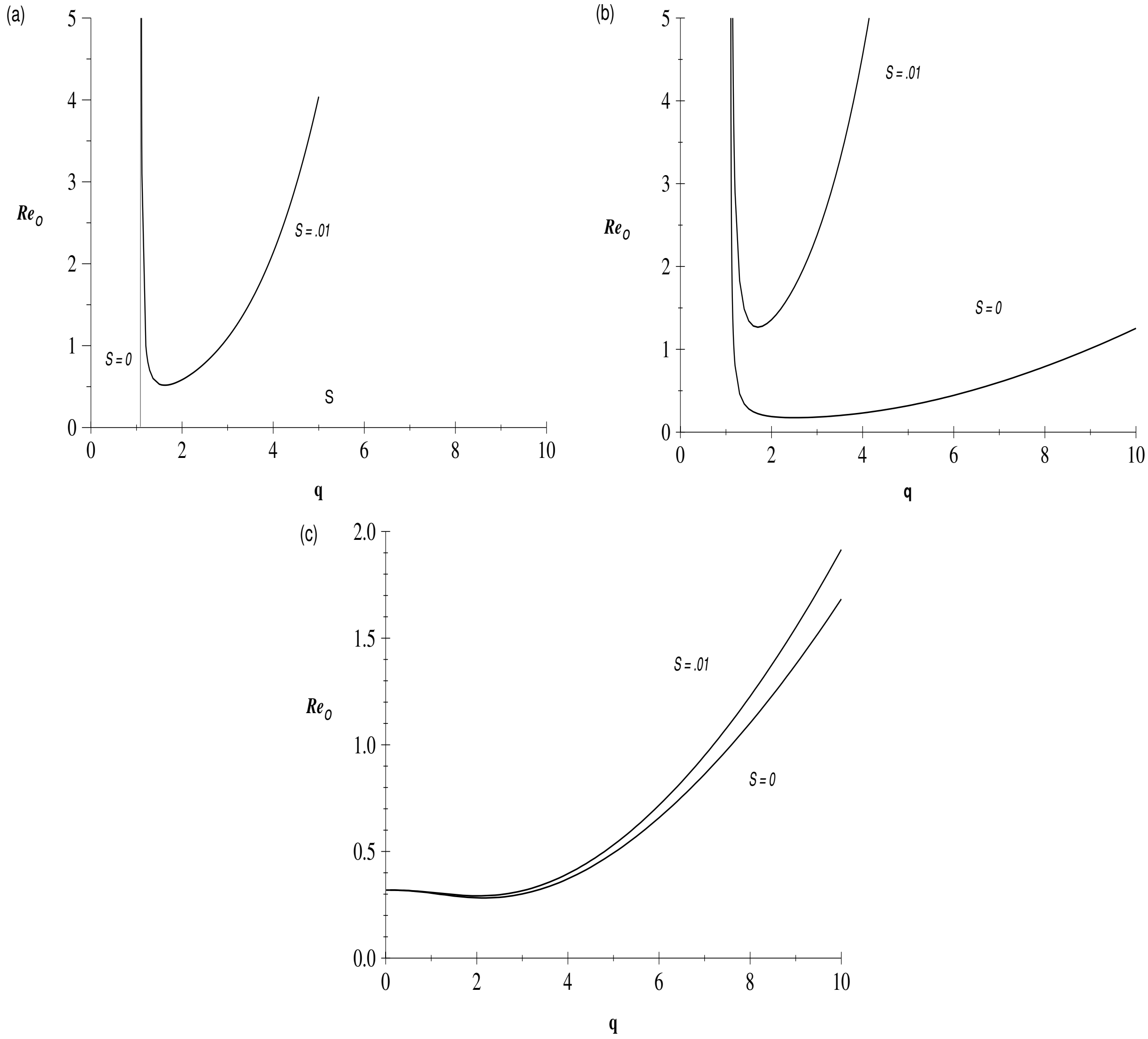

Figure 10: Neutral Reynolds number Re_o versus wavenumber q for Newtonian and Oldroyd-B two-layer flow. Parameters: $r = 1$, $\mathrm{F} = \infty$, $m = 4.$. (a) Newtonians : unstable if $q > 1.09$ for $S = 0$ and $(q_c, \mathrm{Re}_c) = (1.62, .52)$ for $S = .01$. (b) $\epsilon = 3.$, $M_\lambda = 1.2$, $\alpha_k = .9$, $\mathrm{We} = .01$: $(q_c, \mathrm{Re}_c) = (2.5, .175)$ for $S = 0$ and $(q_c, \mathrm{Re}_c) = (1.7, 1.267)$ for $S = .01$. (c)$\epsilon = .3$, $M_\lambda = .8$, $\alpha_k = .9$, $\mathrm{We} = .01$: $\mathrm{Re}_o(q = 0) = .319$, $(q_c, \mathrm{Re}_c) = (2.15, .282)$ for $S = 0$ and $(q_c, \mathrm{Re}_c) = (2., .292)$ for $S = .01$

gives a good approximation of the most critical Reynolds number for the arrangements depicted in the Figs 7d and 7e. Notice that this latter critical Reynolds number is not always the smallest. For example, in the Fig. 10c, the most dangerous Reynolds number is reached for $q = 2.15$. Another interesting feature is the weak influence of the surface tension S on this most critical Reynolds number.

In Figs 11, the critical Reynolds number is reached for the sinuous mode. Therefore, the sinuous mode seems to be the first unstable mode when the Reynolds number increases. This feature is enforced by the surface tension (The difference between the two neutral Reynolds number associated to each mode increase with S). However in the Fig. 11c, the asymptotic neutral Reynolds number is associated to a varicose mode and the nature of the most critical mode changes as the wavenumber increases.

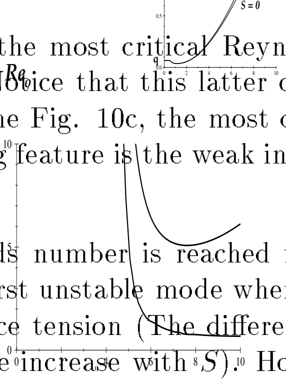

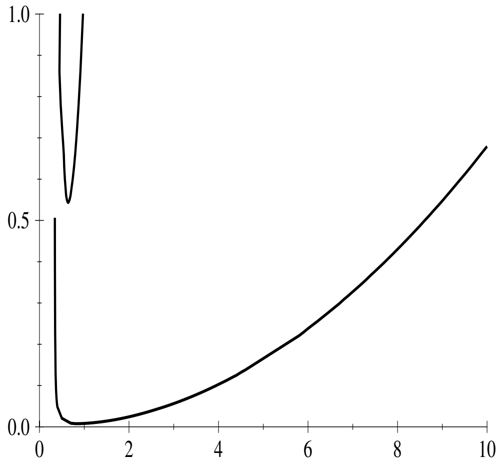

Figure 11: Neutral Reynolds number Re_o versus wavenumber q for an Oldroyd-B three-symmetric layer flow. Parameters: $r = 1$, $\mathrm{F} = \infty$, $\alpha_i = .9$, $\mathrm{We} = .01$. (a) $\epsilon = 3.$, $m = .4$, $M_\lambda = 1.2$: $(q_c, \mathrm{Re}_c) = (.9, .011)$ for $S = 0$ and $(q_c, \mathrm{Re}_c) = (.4, .8)$ for $S = .01$. (b) $\epsilon = .3$, $m = .4$, $M_\lambda = .8$: $(q_c, \mathrm{Re}_c) = (4.8, 7.6)$ for $S = .01$. (c) $\epsilon = .3$, $m = 4.$, $M_\lambda = .8$: $\mathrm{Re}_o(q = 0) = .067$ and $(q_c, \mathrm{Re}_c) = (.6, .06)$ for $S = .0$ and $.01$.

5 Discussion and conclusion

There is a relatively large number of papers concerned with the stability of multilayer Poiseuille flows. They have already examined the interfacial stability of two-layer or three-layer parallel channel flows by means of longwave asymptotic analysis and computation of growth rate for disturbance with modereate wavelength. In this paper, we have followed the same methodology, but in addition to previous studies, we have revisited the asymptotic analysis by using more extensively the additiveness between Newtonian and elastic terms in the expression of the interfacial eigenvalue (the relation (16)). It was also extended to the three-symmetric layer flow which has been studied experimentally [21, 22] and can give a good and easy guideline on the stability of concentric coextrusion [18]. In particular, we take into account of the sinuous modes which are not yet completly studied int the previous works. This new mode sligtly increases the region for which the Poiseuille flow is unstable. A more complete study on the competition between the varicose and sinuous modes will be devoted to a forcomming paper.

We have also summarized in Figs. 7 all asymptotic stable situations at zero Reynolds number for both two-layer and three-symmetrical-layer Poiseuille flow. Thus allow us to exhibit the following properties which give stable situations for three-symmetrical layer (in the meaning that the irregular interfaces are observed more difficultly) :

(i) when the high viscosity component is between the low viscosity ($m < 1$) and whatever the elastic stratification M_λ, it is sufficient to adjust the thicknees ratio ϵ in order to reach a stable situation.

(ii) when the outer layer is less elastic ($M_\lambda < 1$), there exists a thickness ratio ϵ under which the system is asymptotically stable whatever the viscosity ratio m_2.

(iii) when the outer layer is more elastic ($M_\lambda < 1$) and more viscous ($m > 1$), due to the sinuous mode the situation is always unstable whatever the thickness ratio ϵ.

Finally, we point out that the stable arrangements are related to Poiseuille velocity profile and have two different origins :

(i) The Poiseuille velocity profile is convex (see Figs. 2). The stability comes from viscous stratification (in the meaning that this arrangement is stable for Newtonian fluids). The elastic stratification is chosen in order to save this stability (the more elastic fluid has to be in the larger layer). However, if the elastic stratification does not preserve the stability, the Reynolds number can be increased so that the arrangement becomes again asymptotically stable.

(ii) The Poiseuille velocity profile is not convex. The stability is due to the elastic properties. In fact, the elastic stratification has to balance the destabilization due to the viscosity stratification. Therefore, if the Poiseuille velocity profile is not convex and the more elastic fluid is in the thinner layer the arrangement is always unstable.

Of course asymptotic stability does not ensure moderate wavelength stability in the general case. Nevertheless, we found that at zero Reynolds number, the above asymptotically stable configurations remain stable with respect to moderate wavenumber perturbations. It is an important difference with respect to purely Newtonian fluids.

Nevertheless, the previous studies do not show clearly which parameter causes the loss of stability. From an experimental point of view, we can modify very easily the flow rates at the exit of each extruder (namely Q_1 and Q_2 for each fluid). The elasticity or viscosity ratios also depend on the melt extrusion temperature in the feedblock, but this sensitivity varies from polymer to polymer and does not easily allow all possible combinations of viscosity and elasticity ratios. For fixed viscosity and elasticity ratios, a specific thickness ratio ϵ can be choosen by imposing a suitable flow rate ratio Q_2/Q_1. Then, the Reynolds number is modified by changing the two flow rates Q_1 and Q_2 in a such way that the ratio Q_2/Q_1 remains constant. Consequently, it is possible to deal with systems which are destabilized by a Reynolds number increase. In this way, we are in the classical framework where the Reynolds number is the bifurcation parameter. On the contrary, Anturkar [13] and Chen [18] rather determine the critical value of the flow ratio or the volume ratio. However, the layer thickness may be mandated by a product specification and therefore one may not be free to change it. Therefore, this paper is rather focused on stable systems which are destabilized by an increase of the Reynolds number.

As mentioned above, the determination of stable arrangements at zero or small Reynolds number (Re $<<$ 1) can be made by means of asymptotic analysis. We have found that all these stable configurations are destabilized by a small critical Reynolds number. It is important to point out that in our computational examples the critical Reynolds number is always moderate (less than 1) and can be obtained in classical polymer processing conditions. Finally, the critical Reynolds number is reached in two different ways:

(i) if the Poiseuille profile is convex, the critical Reynolds number is reached for a non zero critical wavenumber (q is $O(1)$ in the two-layer case and q depends on ϵ in the three-layer case) and the most critical Reynolds number highly depends on the surface tension. The nonlinear behavior is described by the classical amplitude equation $h_t = \mu h + b|h|^2 h$ and travelling wave pattern is expected on the extruded sheet [30]. Moreover, in the three-symmetrical layer case, it seems that the critical mode is sinuous for viscoelastic case whereas is varicose for purely Newtonian fluid.

(ii) if the Poiseuille profile is not convex, there exists a zero critical wavenumber and therefore the asymptotic analysis can give an estimate of the most critical Reynolds number. Moreover, the surface tension does not play an important role. In this case, the nonlinear behavior is described by the well known Kuramoto-Sivashinsky equation $h_t + h\ h_x + dh_{xx} + sh_{xxxx} = 0$ which can lead to very irregular interfaces [31]. In the case of three symmetrical layer, the longwave critical mode is most of the time the varicose mode.

Acknowledgements

This research has been partially supported by the GDR CNRS 901 ”Rhéologie pour la transformation des polymères fondus”.

References

[1] C.D. Han, Rheology in Polymer Processing, chapter 10, Academic Press (1976).

[2] D.D. Joseph and Y.Y. Renardy, Fundamentals of two-fluid dynamics, Part I: Mathematical Theory and Applications, Springer-Verlag (1992).

[3] R. Sureshkumar and A.N. Beris, Linear stability analysis of viscoelastic Poiseuille flow using Arnoldi-based orthogonalization algorithm, J. Non-Newtonian Fluid Mech., 56 (1995) 151-182.

[4] S. Orszag, Accurate solution of the Orr-Sommerfeld Equation, J. Fluid Mechanics, 50 4 (1971) 689-703.

[5] Y. Saad, Varaitions on Arnoldi's method for computing eigenelements of large unsymetric matrices, Linear Algebra and its Applications, 34 (1980) 269-295.

[6] C.S. Yih, Instability due to viscosity stratification, J. Fluid Mech., 27 (1967) 337-352.

[7] S. G. Yiantsios B. G. Higgins, Linear stability of plane Poiseuille flow of two superposed fluids, Phys. Fluids, 31 (1988) 3225-3238. Erratum Phys. Fluids A1, (1989) 897

[8] F. Charru and J. Fabre, Long waves at the interface between two viscous fluids, Phys. Fluids, 6 (1994) 1223-1235.

[9] B. Khomami, Interfacial stability and deformation of two stratified power law fluids in plane Poiseuille flow, Part I. Stability analysis, J. Non-Newtonian Fluid Mech. 36 (1990) 289-303.

[10] B. Khomami, Interfacial stability and deformation of two stratified power law fluids in plane Poiseuille flow, Part II. Interface deformation, J. Non-Newtonian Fluid Mech. 37 (1990) 19-36.

[11] A. Pinarbasi, A. Liakopoulos, Stability of two-layer Poiseuille flow of Carreau-Yasuda and Bingham-like fluids, , J. Non-Newtonian Fluid Mech. 57 (1995) 227-241.

[12] Y. Renardy, Viscosity and density stratification in vertical Poiseuille flow, Phys. Fluids, 30 (1987) 1638-1648.

[13] N.R. Anturkar, T.C. Papanastasiou and J.O. Wilkes, Linear stability analysis of multilayer plane Poiseuille flow, Phys. Fluids A, 2 (1990) 530-541.

[14] C.-H. Li, Stability of two superposed elasticoviscous Liquids in plane Couette flow, Phys. Fluids, 12 (1969) 531-538.

[15] N.D. Waters and A.M. Keeley, Stability of two stratified non-Newtonian liquids in Couette flow, J. Non-Newtonian Fluid Mech., **24** (1987) 161-181.

[16] N.R. Anturkar, J.O. Wilkes and T.C. Papanastasiou, Stability of multilayer extrusion of viscoelastic liquids, AIChE J. **36** (1990) 710-724.

[17] K.P. Chen, Elastic instability of the interface in Couette flow of viscoelastic liquids, J. Non-Newtonian Fluid Mech. 40 (1991) 261-267.

[18] K.P. Chen, Interfacial instability due to elastic stratification in concentric coextrusion of two viscoelastic fluids, J. Non-Newtonian Fluid Mech. 40 (1991) 155-175.

[19] Y. Renardy, Stability of the interface in two-layer Couette flow of an upper convected Maxwell fluid, J. of Non-Newtonian Fluid Mech., 28 (1988) 99-115.

[20] Y. Y. Su and B. Khomami, Interfacial stability of multilayer viscoelastic fluids in slit and converging channel dies geometries, J. Rheol., 36 (1992) 357-387.

[21] C. D. Han and R. Shetty, Studies on multilayer film coextrusion I. The rheology of flat film coextrusion, Polym. Eng. Sci., 16 (1976) 697-705.

[22] C. D. Han and R. Shetty, Studies on multilayer film coextrusion II. Interfacial instability in flat film coextrusion, Polym. Eng. Sci., 18 (1978) 180-186.

[23] N.R. Anturkar, T.C. Papanastasiou and J.O. Wilkes, Estimation of critical stability parameters by asymptotic analysis in multilayer extrusion, Polym. Eng. Sci., 33 (1993) 1532-1539.

[24] N.R. Anturkar, T.C. Papanastasiou and J.O. Wilkes, Stability of coextrusion through converging dies, J. Non-Newtonian Fluid Mech. 41 (1991) 1-25.

[25] B. Khomami, G. M. Wilson, An experimental investigation of interfacial instability in superposed flow of viscoelastic fluids in a converging/diverging channel geometry, J. Non-Newtonian Fluid Mech., 58 (1995) 47-65.

[26] E.J. Hinch, O.J. Harris and J.M. Rallison, The instability mechanism for two elastic liquids being co-extruded, J. Non-Newtonian Fluid Mech., 43 (1992) 311-324.

[27] M. Renardy and Y. Renardy, Linear Stability of plane Couette Flow of an upper convected Maxwell fluid, J. Non-Newtonian Fluid Mech., 22 (1986) 23-33.

[28] B.S. Tilley, S.H. Davis and S.G. Bankoff, Linear stability theory of two-layer fluid in an inclined channel, Phys. Fluids, 6 (1994) 3906-3922.

[29] N. Nayar and J. Ortega, Computation of selected eigenvalues of generalized eigenvalue problems, J. of Computational Physics, 108 (1993) 8-14.

[30] Y. Renardy, Weakly nonlinear behavior of periodic disturbances in two-layer plane channel flow of upper-convected Maxwell liquids, J. of Non-Newtonian Fluid Mech., 56 (1995) 101-126.

[31] H.-C. Chang, Wave evolution on fallling film, Ann. Rev. Fluid Mech., 26 (1994), 103-136.

A Functions c_0, J_1, J_2, J_3, J_4 and J_5 in the case A

$$c_0 = f(\epsilon, m) = 1 + 2\,\frac{\epsilon\,(m - \epsilon^2)\,(m - 1)}{d_0}$$

with

$$d_0 = m^2 + 2\,\epsilon\,m\,(2\,\epsilon^2 + 3\,\epsilon + 2) + \epsilon^4$$

$$\begin{aligned}
J_1 &= \frac{(m - \epsilon^2)\,(m - 1)\,f_1(\epsilon, m)}{420\,m^2\,d_0^3\,(\epsilon + 1)^2} \\
f_1 &= (6\,\epsilon + 1)\,m^7 + (-2\,\epsilon - 9\,\epsilon^2 - 120\,\epsilon^3 - 88\,\epsilon^4)\,m^6 \\
&\quad + (32\,\epsilon^2 + 344\,\epsilon^3 + 821\,\epsilon^4 + 1426\,\epsilon^5 + 1096\,\epsilon^6 + 224\,\epsilon^7)\,m^5 \\
&\quad + (408\,\epsilon^4 + 1642\,\epsilon^5 + 3667\,\epsilon^6 + 3424\,\epsilon^7 + 1240\,\epsilon^8 + 224\,\epsilon^9)\,m^4 \\
&\quad + (224\,\epsilon^5 + 1240\,\epsilon^6 + 3424\,\epsilon^7 + 3667\,\epsilon^8 + 1642\,\epsilon^9 + 408\,\epsilon^{10})\,m^3 \\
&\quad + (224\,\epsilon^7 + 1096\,\epsilon^8 + 1426\,\epsilon^9 + 821\,\epsilon^{10} + 344\,\epsilon^{11} + 32\,\epsilon^{12})\,m^2 \\
&\quad + (-88\,\epsilon^{10} - 120\,\epsilon^{11} - 9\,\epsilon^{12} - 2\,\epsilon^{13})\,m + \epsilon^{14} + 6\,\epsilon^{13}
\end{aligned}$$

$$\begin{aligned}
J_2 &= \frac{\epsilon^3\,(m - \epsilon^2)\,(m - 1)\,f_2(\epsilon, m)}{420\,m^2\,d_0^3\,(\epsilon + 1)^2} \\
f_2 &= (224 + 1043\,\epsilon + 1486\,\epsilon^2 + 672\,\epsilon^3)\,m^5 \\
&\quad + (392\,\epsilon + 2086\,\epsilon^2 + 3021\,\epsilon^3 + 1080\,\epsilon^4 - 272\,\epsilon^5)\,m^4 \\
&\quad + (224\,\epsilon^2 + 1512\,\epsilon^3 + 2344\,\epsilon^4 + 646\,\epsilon^5 - 444\,\epsilon^6 + 16\,\epsilon^7)\,m^3 \\
&\quad + (224\,\epsilon^4 + 424\,\epsilon^5 - 60\,\epsilon^6 - 222\,\epsilon^7 + 120\,\epsilon^8 + 32\,\epsilon^9)\,m^2 \\
&\quad + (-\,88\,\epsilon^7 - 120\,\epsilon^8 - 9\,\epsilon^9 - 2\,\epsilon^{10})\,m + 6\,\epsilon^{10} + \epsilon^{11}
\end{aligned}$$

$$J_3 = \frac{\epsilon^3 \ (m+\epsilon)}{3 \ d_0}$$

$$J_4 = \frac{-2 \ \epsilon \ (m \ - \ \epsilon^2) \ (m \ - \ 1) \ (m \ + \ \epsilon) \ f_4(\epsilon, m)}{3 \ m \ d_0^2 \ (\epsilon \ + \ 1)^2}$$

$$f_4 = m^3 + (-2 \ - \ 5 \ \epsilon \ - \ 8 \ \epsilon^2 \ - \ 2 \ \epsilon^3) \ m^2 + (-2 \ \epsilon^2 \ - \ 5 \ \epsilon^4 \ - \ 8 \ \epsilon^3 \ - \ 2 \ \epsilon^5) \ m \ + \ \epsilon^5$$

$$J_5 = \frac{(m \ - \ \epsilon^2) \ f_5(\epsilon, m)}{3 \ \ m \ d_0^3(\epsilon \ + \ 1)^2}$$

$$\begin{aligned} f_5 = {} & (3 + 16 \ \epsilon + 11 \ \epsilon^2 - 12 \ \epsilon^3 - 12 \ \epsilon^4) \ m^6 \\ & + (8 \ \epsilon \ + 99 \ \epsilon^2 \ + \ 242 \ \epsilon^3 \ + \ 287 \ \epsilon^4 + \ 184 \ \epsilon^5 \ + \ 60 \ \epsilon^6) \ m^5 \\ & + (- \ 32 \ \epsilon^2 \ - \ 94 \ \epsilon^3 \ - \ 142 \ \epsilon^4 \ - \ 96 \ \epsilon^5 \ - \ 26 \ \epsilon^6 \ + \ 16 \ \epsilon^7 \ - \ 4 \ \epsilon^8) \ m^4 \\ & + (-16 \ \epsilon^3 \ - 88 \ \epsilon^4 - \ 216 \ \epsilon^5 \ - \ 254 \ \epsilon^6 \ - \ 188 \ \epsilon^7 \ - \ 66 \ \epsilon^8 - \ 40 \ \epsilon^9 \ - \ 12 \ \epsilon^{10}) \ m^3 \\ & + (123 \ \epsilon^8 - 32 \ \epsilon^6 + 176 \ \epsilon^9 + 28 \ \epsilon^7 + 79 \ \epsilon^{10} + 12 \ \epsilon^{11} - 16 \ \epsilon^5) \ m^2 \\ & + (-8 \ \epsilon^8 - 16 \ \epsilon^9 \ + \ 11 \ \epsilon^{10} \ + \ 10 \ \epsilon^{11} \ + \ 3 \ \epsilon^{12}) \ m \ + \ 2 \ \epsilon^{11} \end{aligned}$$

B Functions c_0, J_1, J_2, J_4 and J_5 in the case B

B.1 Varicose mode

$$c_0 = f(\epsilon, m) = 1 \ + \ \frac{\epsilon \ (3 \ + \ 2\epsilon) \ (m-1)}{(2+\epsilon) \ d_0}$$

with

$$d_0 = \epsilon^3 \ + \ 3\epsilon^2 \ + \ 3\epsilon \ + \ m$$

$$J_1 = \frac{(m-1) \ f_1(\epsilon,m)}{420 \ m(2+\epsilon)^2 \ d_0^3}$$

$$\begin{aligned} f_1 = {} & (32 + 96\epsilon) m^4 + (272 \ \epsilon^2 + 96\epsilon - 464\epsilon^3 - 352\epsilon^4) \ m^3 \\ & +(252 \ \epsilon^2 + \ 1428 \ \epsilon^3 + \ 980 \ \epsilon^4 + \ 940 \ \epsilon^5 + \ 224 \ \epsilon^7 + \ 896 \ \epsilon^6) \ m^2 \\ & +(882 \ \epsilon^4 + \ 212 \ \epsilon^8 + \ 642 \ \epsilon^6 + \ 702 \ \epsilon^7 \ + 714 \ \epsilon^5) \ m \\ & 378 \ \epsilon^5 \ + 120 \ \epsilon^9 \ + 342 \ \epsilon^8 \ + 438 \ \epsilon^7 \ + 504 \ \epsilon^6 \ + 10 \ \epsilon^{10} \end{aligned}$$

$$J_2 = \frac{(m-1) \ \epsilon^3 \ f_2(\epsilon, m)}{420 \ m(2+\epsilon)^2 \ d_0^3}$$

$$\begin{aligned} f_2 = {} & (672 + \ 2212\epsilon + \ 2172 \ \epsilon^2 + \ 672 \ \epsilon^3) m^2 \\ & +(882 \ \epsilon \ + \ 3234 \ \epsilon^2 + \ 3477 \ \epsilon^3 \ + \ 1262 \ \epsilon^4 + \ 72 \ \epsilon^5) m \\ & + \ 378 \ \epsilon^2 \ + \ 1449 \ \epsilon^3 \ + \ 1698 \ \epsilon^4 \ + \ 762\epsilon^5 + \ 120 \ \epsilon^6 \ + \ 10 \ \epsilon^7 \end{aligned}$$

$$J_4 = \frac{-\epsilon\ (m - 1)\ (4\ m + 3\ \epsilon)(\ 2\ m - 2 - (1 + \epsilon)^3)}{3\ (2 + \epsilon)^2\ d_0^2}$$

$$J_5 = \frac{f_5(\epsilon, m)}{(2+\epsilon)^2\ d_0^3}$$

$$\begin{aligned} f_5 = {} & (4 + 16\ \epsilon + 4\ \epsilon^2 - 8\ \epsilon^3 - 4\ \epsilon^4)\ m^3 \\ & +(8\ \epsilon + 78\ \epsilon^2 + 112\ \epsilon^3 + 72\ \epsilon^4 + 24\epsilon^5 + 4\epsilon^6)\ m^2 \\ & +(-\ 24\ \epsilon^2 - 27\ \epsilon^3 - 20\ \epsilon^4 - 19\ \epsilon^5 - 15\ \epsilon^6 - 6\ \epsilon^7 - \epsilon^8)\ m \\ & -\ 9\ \epsilon^3 - 18\epsilon^4 - 21\ \epsilon^5 - 15\ \epsilon^6 - 6\ \epsilon^7 - \epsilon^8 \end{aligned}$$

B.2 sinuous mode

$$c_0 = 1 + \frac{\epsilon\,(m-1)}{(2+\epsilon)\,(\epsilon+m)}$$

$$J_1 = \frac{(m-1)\,\epsilon^2\,(1+\epsilon)\,f_1(\epsilon,m)}{30\,m\,(2+\epsilon)^2\,(\epsilon+m)^3}$$

$$f_1 = \epsilon^3 + 7\,\epsilon^2\,m + 10\,m^2 + 16\,\epsilon\,m^2$$

$$J_4 = \frac{(m-1)\,\epsilon\,(1+\epsilon)\,(\epsilon+4\,m)}{3\,(2+\epsilon)^2\,(\epsilon+m)^2}$$

$$J_5 = \frac{(1+\epsilon)\,f_5\,(\epsilon,m)}{3\,(2+\epsilon)^2\,(\epsilon+m)^3}$$

$$f_5 = -\epsilon^3 + (-8\,\epsilon^2 + \epsilon^3)\,m + (8\,\epsilon + 8\,\epsilon^2)\,m^2 + (12 + 4\,\epsilon)\,m^3$$